



UNIVERSITY OF LEEDS

This is a repository copy of *Dichroic Calcite Reveals the Pathway from Additive Binding to Occlusion*.

White Rose Research Online URL for this paper:

<https://eprints.whiterose.ac.uk/175432/>

Version: Accepted Version

---

**Article:**

Green, DC orcid.org/0000-0002-0578-2369, Darkins, R, Marzec, B et al. (6 more authors) (2021) Dichroic Calcite Reveals the Pathway from Additive Binding to Occlusion. *Crystal Growth & Design*. acs.cgd.1c00068. ISSN 1528-7483

<https://doi.org/10.1021/acs.cgd.1c00068>

---

© 2021 American Chemical Society. This is an author produced version of a journal article published in *Crystal Growth & Design*. Uploaded in accordance with the publisher's self-archiving policy.

**Reuse**

Items deposited in White Rose Research Online are protected by copyright, with all rights reserved unless indicated otherwise. They may be downloaded and/or printed for private study, or other acts as permitted by national copyright laws. The publisher or other rights holders may allow further reproduction and re-use of the full text version. This is indicated by the licence information on the White Rose Research Online record for the item.

**Takedown**

If you consider content in White Rose Research Online to be in breach of UK law, please notify us by emailing [eprints@whiterose.ac.uk](mailto:eprints@whiterose.ac.uk) including the URL of the record and the reason for the withdrawal request.



[eprints@whiterose.ac.uk](mailto:eprints@whiterose.ac.uk)  
<https://eprints.whiterose.ac.uk/>

## Dichroic Calcite Reveals the Pathway from Additive Binding to Occlusion

David C. Green<sup>a†\*†</sup>, Robert Darkins<sup>b‡\*</sup>, Bartosz Marzec<sup>a</sup>, Mark A. Holden<sup>a,c§</sup>, Ian J. Ford<sup>b</sup>, Stanley W. Botchway<sup>d</sup>, Bart Kahr<sup>e</sup>, Dorothy M. Duffy<sup>b</sup> and Fiona C. Meldrum<sup>a\*</sup>

<sup>a</sup>School of Chemistry, University of Leeds, Woodhouse Lane, Leeds, LS2 9JT, United Kingdom.

<sup>b</sup>London Centre for Nanotechnology, University College London, Gower Street, London, WC1E

6BT, United Kingdom. <sup>c</sup>School of Physics and Astronomy, University of Leeds, LS2 9JT, United

Kingdom. <sup>d</sup>Central Laser Facility, Science and Technology Facilities Council, Research Complex at

Harwell, Rutherford Appleton Laboratory, Didcot OX11 0QX, United Kingdom. <sup>e</sup>Molecular Design

Institute, NYU Department of Chemistry, 100 Washington Square East, New York, NY 10003-

6688, United States of America.

**Keywords:** *calcium carbonate, molecular dynamics, atomic force microscopy, dye, optical properties, crystallization*

### Abstract

Organic additives play key roles in controlling the precipitation of calcium carbonate in biology, the environment and industry, where they can direct polymorphism, alter crystal morphologies and sometimes even become occluded, modifying bulk properties. However, significant questions remain regarding the pathway from adsorption on the crystal surface to occlusion. Here, the optical properties of calcite crystals grown in the presence of the dye Congo red are used to characterize the organization of the additives within the crystal. Complemented by

analysis of surface adsorption through in situ atomic force microscopy, molecular simulations and changes in crystal morphologies, we show that the occluded dye molecules are randomly oriented under fast growth conditions, but that slow growth engenders ordering of the dye within islands, whose orientation is determined by the dye/terrace interaction free energy. The islands are subsequently overgrown such that their internal structure is preserved. These results reveal that the occlusion of organic macromolecules into calcite can be understood by thermodynamics operating at the adsorption stage. This new insight will ultimately enable the design of additives to give specific material properties.

## **1. Introduction**

Soluble additives are widely used to control crystallization, where their ability to produce particles with specific morphologies, sizes and polymorphs is well-documented.<sup>1-3</sup> The mechanisms by which these additives interact with growing crystals have therefore attracted considerable attention,<sup>4-7</sup> where changes in crystal morphology can provide a signature of the interaction between an additive and the crystal surface. When a crystal displays a number of symmetry-independent faces, additives will bind selectively to these, changing the relative sizes of these faces in the product crystal morphology.<sup>8</sup> Calcite ( $\text{CaCO}_3$ ) crystals grown in solution, on the other hand, only express {104} faces in solution. However, additives can still alter the crystal morphology by binding selectively to the acute or obtuse steps on the {104} faces,<sup>9-13</sup> leading to the formation of new, rough pseudo-faces.

Additive-binding to a crystal surface is a dynamic process, where adsorbed additives can either desorb or become incorporated within the crystal if they are engulfed by the advancing steps.<sup>14</sup> For instance, the incorporation of proteins within single crystals of calcite, which is a crucial process in biomineralization, endow structures with enhanced mechanical properties.<sup>15, 16</sup> Substitution of calcium ions by trace elements of identical charge leads to the formation of a traditional solid solution,<sup>17-19</sup> while small molecules such as amino acids<sup>20-22</sup> can also behave as solutes, replacing both calcium and carbonate ions in the crystal structure.<sup>21</sup> In contrast, larger additives such as protein aggregates,<sup>23-25</sup> copolymer micelles,<sup>15</sup> polymer-functionalized inorganic nanoparticles,<sup>26-28</sup> latex particles<sup>29</sup> and vesicles<sup>30, 31</sup> are incorporated as second-phase particles. This incorporation of additives is also known as occlusion.

Understanding how occlusion occurs is challenging. The locations of individual particulate additives can be readily determined using electron microscopy,<sup>15, 29, 32, 33</sup> tomography techniques,<sup>28, 34, 35</sup> and even super-resolution microscopy.<sup>35</sup> Molecular-scale additives, however, are far harder to characterize. Techniques such as Raman microscopy,<sup>36</sup> confocal fluorescence microscopy,<sup>37-40</sup> and cathodoluminescence<sup>17, 18</sup> provide information on the global locations of occluded additives, but can only be applied to species with suitable signatures. Single crystal and powder X-ray diffraction (XRD) analysis can be applied to any crystal where occlusion is accompanied by lattice distortions that may reflect the location of the additive.<sup>25, 41-43</sup>

Much of our knowledge about the incorporation of molecular additives within single crystals has therefore come from the use of colored or fluorescent dyes, where these are easily visualized

within individual crystals.<sup>40, 44</sup> Many locate within specific zones, giving information about crystal/additive interactions and the local environments of the dyes.<sup>45, 46</sup> Furthermore, some colored dye molecules impart anisotropic optical properties to the crystals in which they are incorporated. If molecules of a suitable dye are oriented into growth sectors into which they have been overgrown in non-random orientations – such that the crystal exhibits orientation-dependent optical properties when viewed with polarized light – it is possible to determine the orientations of the individual molecules with respect to the crystal structure.<sup>40</sup>

This article describes a study of calcite growth in the presence of the colored dye Congo red. Congo red was selected for the study as it is one of the few colored dyes reported to occlude within calcite, and AFM studies of binding to calcite {104} faces have indicated preferred orientation on the terraces. The product crystals are dichroic and have optical properties that vary with the polarization plane of the probing light. This dichroism provides key insight into the orientation of the dye molecules occluded within the crystal, while the dye interactions with the calcite surface were revealed by a combination of atomic force microscopy (AFM), an analysis of crystal morphology, and molecular simulations. Taken together, a comprehensive picture emerges of how Congo red molecules interact with and occlude within calcite crystals.

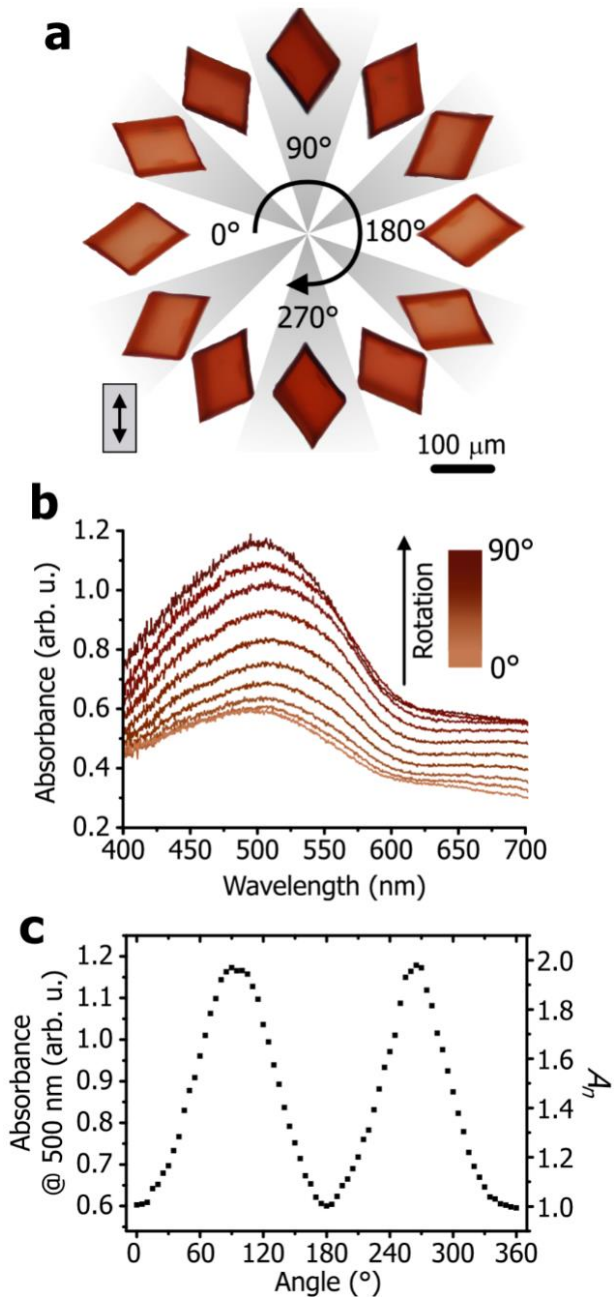


**Figure 1. Overgrowth of calcite crystals in the presence of Congo red.** (a) Optical micrographs of overgrown  $\text{CaCO}_3$  seeds grown in solution containing  $[\text{Ca}^{2+}] = [\text{HCO}_3^-] = 5 \text{ mM}$  taken at different angles with respect to the plane of polarized light. (b) Absorbance spectra obtained from calcite at different rotations with respect to the plane of polarized light, where  $0^\circ = [010]$  and polarized light are parallel and perpendicular. (c) Absorbance values at 500 nm vs angle. These values are also plotted as  $A_n$ , and reveal a dichroic ratio,  $R$ , of 1.97 (top of the peak).

## 2. Results

### 2.1 Influence of Congo red on Calcite Growth

Congo red can alter the morphology of calcite, roughen its surface and incorporate into the bulk. All three of these effects were exhibited by calcite single crystals generated by a seeded growth method, where a glass slide supporting 50-100  $\mu\text{m}$  calcite seeds was immersed in an aqueous solution of composition  $[\text{CaCl}_2] = [\text{NaHCO}_3] = 5 \text{ mM}$  and  $[\text{Congo red}] = 20 \mu\text{M}$ , and growth was allowed to proceed for 16 h (Figure S1). 20 mM was selected as lower concentrations led to poor incorporation while higher concentrations inhibited growth and significantly altered the crystal morphologies.

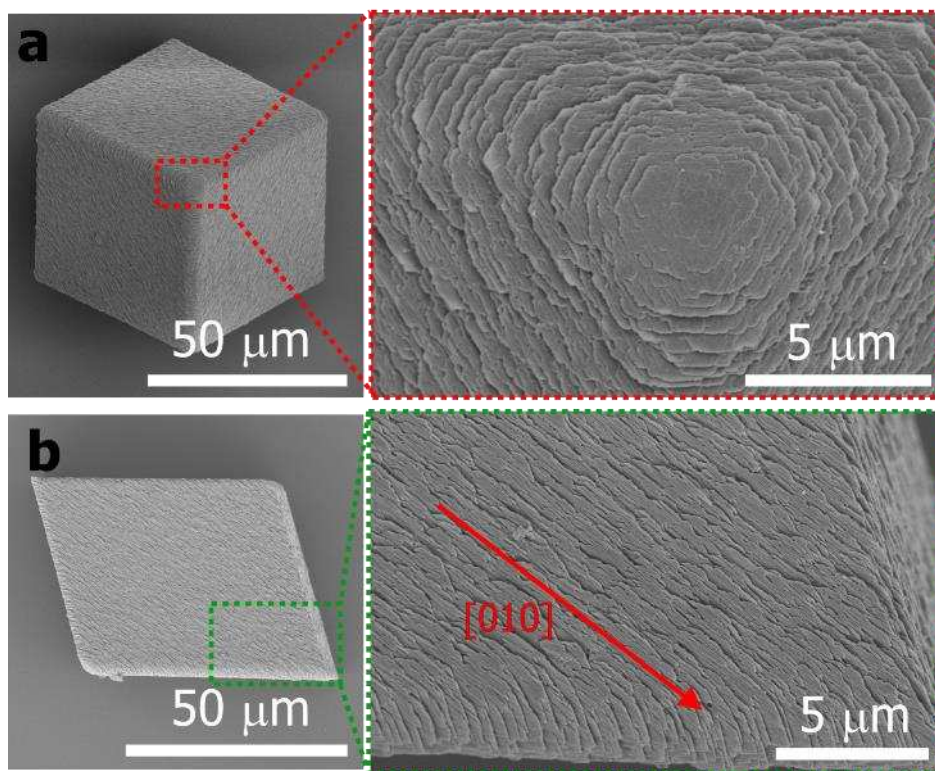


**Figure 2. Morphological effects of Congo red on calcite.** SEM micrographs of overgrown calcite crystals in (001)-up (a) and (104)-up (b) orientation. Higher magnification micrographs showing overexpressed (001) facets (red box, a); and surface striations oriented with calcite's  $\langle 010 \rangle$  axes (green box, b) are shown.

The overgrowth was confirmed as calcite with Raman spectroscopy (Figure S2); and the product crystals were orange/red in color (Figure 1a). Confocal laser fluorescence microscopic (CLFM) analysis showed that the Congo red was incorporated into the overgrown section, and not simply adsorbed onto the calcite surface (Figure S3). The color was somewhat more intense in the outer part of the crystal, where this may derive from the higher dye/ $\text{Ca}^{2+}$  ratio that occurs before growth terminates, or a combination of these effects.

The morphology gave way to a (001) facet and flattened obtuse edges (Figure 2a). This morphology change provides information about the interaction of the additives with the crystal surface. Due to the trigonal symmetry of the calcite crystal, the steps lie at either an acute or obtuse angle to the crystal faces (see Figure 6). Many additives bind selectively to one step geometry, which gives rise to characteristic changes in the crystal morphology.<sup>47</sup> The morphological changes induced by Congo red are indicative of preferential binding to the obtuse over the acute steps.<sup>48</sup> Furthermore, pronounced surface striations ran parallel to  $\langle 010 \rangle$  (Figure 2b), indicating a substantial binding of Congo red to the terraces along that direction that impedes crystal overgrowth and results in a step pile-up.

## **2.2 Optical Properties of Dyed Calcite Crystals**

The Congo red-dyed crystals were dichroic in polarized light. The optical density of the mixed crystals varied with respect to the plane of polarized light normally incident on {104} (Figure 1a). Images of the crystal at different degrees of orientation were recorded. The orientation with the

smallest optical density was defined as  $0^\circ$ , corresponding to the  $\langle 42\bar{1} \rangle$  axis. Mean RGB values were obtained from each optical micrograph. The proportional change in the intensity of the red component was small as compared to those of the green and blue components over a full rotation (Figure S4). This was further demonstrated by plotting the relative red intensity, obtained by dividing the red value by the sum of all RGB values, as a function of the rotation angle (Figure S4). These data were also verified against absorbance spectra (Figure 1b), where the absorbance at 500 nm was plotted as a function of the crystal orientation. An oscillatory variation is observed, where the highest absorbance at 500 nm corresponds to the strongest red color (Figure 1c).

This linear dichroism exhibited by calcite/Congo red crystals demonstrates that the occluded dye molecules have an anisotropic orientation with respect to the calcite crystal structure. The Congo red chromophore absorbs light most strongly at 500 nm when the plane of polarized light is parallel to the molecular long axis.<sup>49</sup> The most intense color was observed when the plane of polarized light was parallel to the  $\langle 010 \rangle$  axis of the crystal, which was identified based on the external morphology of the macroscopic crystal sample. The variation in absorbance upon rotation of the dyed crystal can be quantified by the dichroic ratio,  $R$ , which is the ratio of the maximum absorbance to the minimum absorbance at 500 nm. If the dyes were oriented isotropically within the crystal then  $R$  would be unity, whereas  $R$  would be infinite if each dye molecule was perfectly collinear with either the  $\langle 010 \rangle$  or  $\langle 42\bar{1} \rangle$  axes.  $R$  peaked at 1.97 when the electric field of the polarized light input was parallel to  $\langle 010 \rangle$ . If all the incorporated dye molecules share the same orientation, the  $R$  value measured corresponds to orientations of  $\pm 35^\circ$  to  $\langle 010 \rangle$ .

### 2.3 In Situ Atomic Force Microscopy

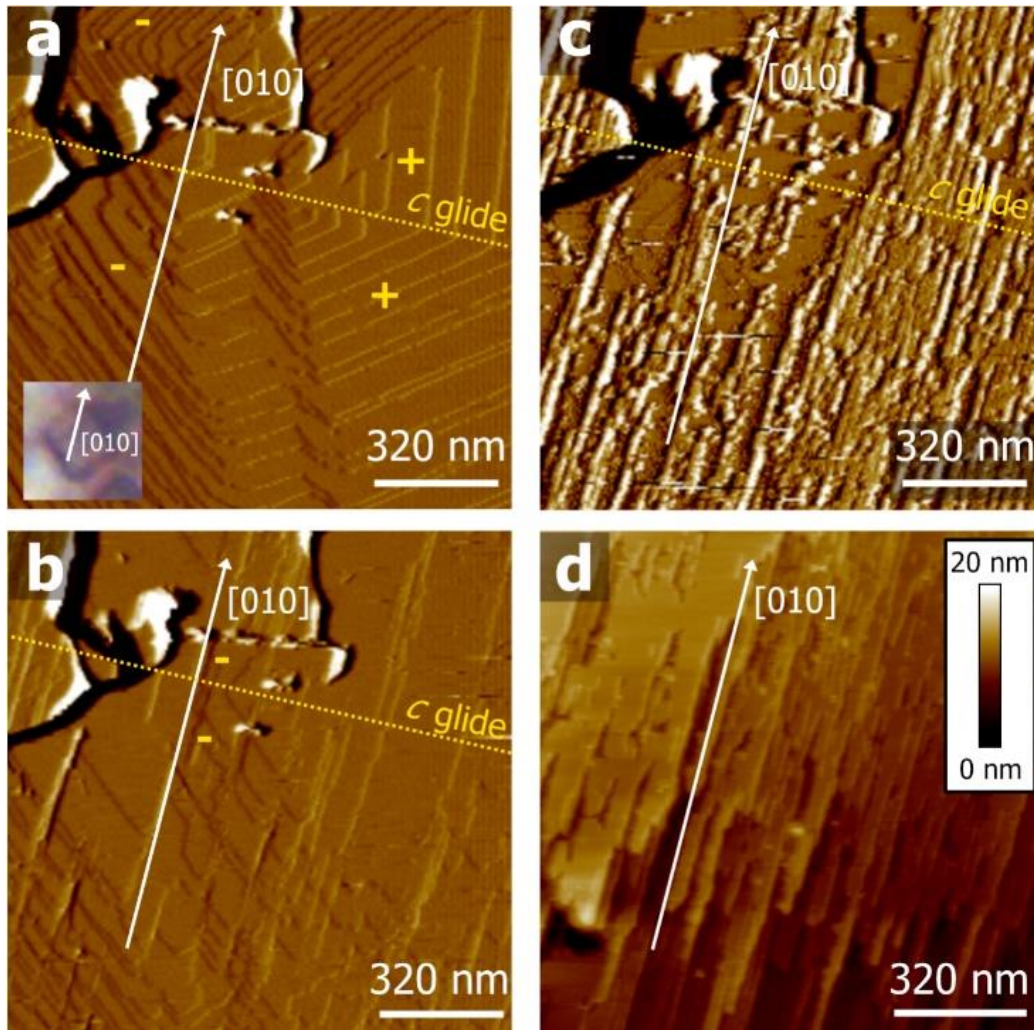


**Figure 3: AFM analysis of Congo red-modified calcite growth.** AFM micrographs of calcite surfaces before (a) and after (b, c and d) the addition of Congo red during growth. Under slow AFM growth conditions, calcite grows as hillocks, which are composed of acute and obtuse steps (a). Deflection image taken within 2 minutes of dye addition, and with a relatively high contact force, showing that after the addition of Congo red, obtuse steps disappear, replaced by a new step edge co-directional with calcite's  $\langle 010 \rangle$  axis (b). Deflection image taken 6 minutes after dye addition with a lower contact force, showing tape-like Congo red "islands" formed behind new step edges (c). Height image taken 39 minutes after dye addition, showing that the surface is covered in parallel steps, aligned with calcite's  $\langle 010 \rangle$  axis (d). The dye islands are observed at the step edges.

The interaction of Congo red with the growing calcite surface was studied using *in situ* AFM. Growth solutions were selected to provide stable, slow growth conditions that can be studied on an AFM time-scale. Calcite grows *via* a step growth mechanism under these conditions, with steps emanating from screw dislocations present on the {104} faces (Figure 3a). Contact mode AFM was performed while flowing supersaturated calcium carbonate solutions over seed crystals at 0.3 mL min<sup>-1</sup>. Addition of Congo red transformed the obtuse steps into [010] steps but had no apparent effect on the acute steps (Figure 3b), providing conclusive evidence that Congo red binds preferentially to the obtuse steps.<sup>50</sup> Over a period of minutes, 20-30 nm wide and 1-4.5 nm high tape-like islands of Congo red formed on the terraces (Figure 3c), leading to a pile-up of steps parallel to [010] (Figure 3d).

## 2.4 Influence of Crystal Growth Conditions

Experiments were conducted to explore the influence of the crystallization conditions on the formation of dichroic calcite/Congo red crystals. The dyed calcite crystals were precipitated using experimental conditions that generate different initial supersaturation values,  $S$ : (1) the ammonium diffusion method (ADM), in which a 10 mM calcium chloride solution was exposed to ammonium carbonate vapor ( $S \approx 35$ ),<sup>51</sup> (2) the direct method (DM) in which a 5 mM supersaturated solution was prepared by mixing calcium chloride and sodium carbonate solutions ( $S \approx 21$ ), and (3) the Kitano method, in which calcium carbonate precipitates on release of CO<sub>2</sub> from a supersaturated solution of calcium bicarbonate<sup>52</sup> ( $S \approx 10$ ). In all cases, the Congo red concentration was fixed at 20 μM.

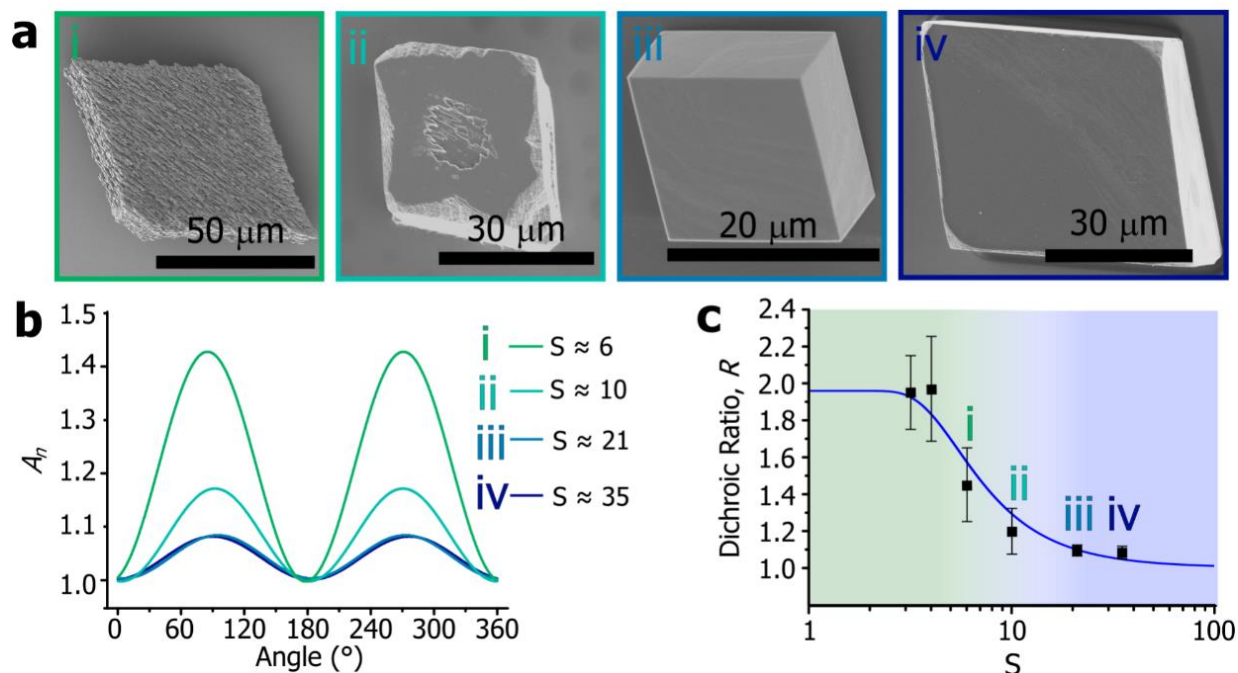


**Figure 4: The coincidence of dichroism and surface roughening.** (a) Scanning electron micrographs of calcite/Congo red crystals grown by 10 mM overgrowth (i), Kitano (ii), DM (iii), and ADM (iv). (b)  $A_n$  vs angle plots prepared from absorbance spectroscopy data obtained from calcite crystals prepared under the same conditions as those stated in a. (c) The dichroic ratio as a function of supersaturation, where the black squares are experimental measurements and the blue curve is a theoretical fit.

Calcite/Congo red crystals precipitated using the ADM and DM methods were principally unmodified rhombohedra with minimal surface roughness, while the Kitano method yielded crystals with weakly modified rhombohedral morphologies and some surface roughening (Figure 4a). All were red/orange, indicating occlusion of the dye. There was no evidence of sectoral zoning which could be expected from step-specific interactions (Figure S5).<sup>45</sup> Confocal laser fluorescence microscopy (CLFM) data suggested that Congo red was incorporated homogeneously in the outermost regions of calcite, leaving a less-occupied core (Figure S6). This

indicates that occlusion and shape modification was most significant during latter-stage, slow growth.<sup>53</sup>

No dichroism was observed in any of these crystals when they were viewed down the  $\langle 001 \rangle$  axis, but weak dichroism was recorded perpendicular to the  $\{104\}$  faces (Figures S4 and S5). Dichroic ratios ( $R$ ) of 1.08, 1.10 and 1.20 were obtained from absorbance spectroscopy data for the ADM, DM and Kitano samples, respectively, which suggests that dichroism increases as the supersaturation decreases (Figure 4b and 4c). This trend was also true in overgrowth experiments, where greater surface roughness (Figure 2 versus Figure 4a), but weaker dichroism, was observed when crystals were precipitated from 10 mM ( $S \approx 6$ ) rather than 5 mM ( $S \approx 4$ ) solutions, yielding  $R = 1.45$  and  $1.97$ , respectively. Reducing the supersaturation further with a 4 mM ( $S \approx 3$ ) solution produced no further increase in  $R$ , suggesting that 1.97 is the maximum attainable value by solution precipitation (Figure 4c).

At much higher Congo red concentrations (100  $\mu\text{M}$ ), calcite precipitated under DM conditions became so disrupted that large plate-like calcite structures formed due to the over-expression of the (001) face (Figure S7). Likewise, *de novo* calcite/Congo red crystals precipitated from low supersaturation overgrowth experiments were so morphologically disrupted that it was impossible to analyze them for their dichroic behavior. Therefore, to investigate such low supersaturations, a seeded method was used to ensure that a distinct crystal morphology was obtained.

We propose that the dichroism diminishes with increasing supersaturation because faster crystal growth traps dye molecules within the crystals in metastable orientations. A simplified theoretical model was developed on this basis whereby an ensemble of incorporating dyes is assumed to adsorb onto a step with an initially isotropic distribution. This isotropic orientation distribution then decays toward a preferred orientation with a characteristic timescale while the local step advances at a speed dependent on the supersaturation. Once the step has advanced by a predefined molecular length-scale, the dyes become kinetically trapped with their orientation distribution preserved. This model predicts a sigmoidal dependence of dichroic ratio on the log-supersaturation and has two free parameters: one that determines the maximum  $R$ , and another that offsets the curve along the  $S$ -axis. While the model is agnostic about the processes responsible for organizing the dyes, fitting it to the experimental data (Figure 4c) produces a reasonable fit and reveals that the organization occurs over a timescale of approximately milliseconds.

## 2.5 Molecular Simulations

In an effort to identify the significance of the preferred dye orientation, molecular dynamics simulations of a single Congo red molecule adsorbed at the calcite (104)/water interface were performed. The molecule lies in the plane of the calcite terrace but separated by two hydration layers (Figure S8), consistent with simulations of the similarly-structured dye benzopurpurine 4B.<sup>54</sup> The free energy as a function of dye orientation was computed using umbrella sampling, and the resulting Boltzmann probability distribution shows a clear preference to lie at  $28^\circ$  to the [010] direction (Figure 5), with a free energy that varies by 3.3 kcal/mol with respect to

orientation. The presence of water layers between the dye and calcite surface suggests that the dye aligns so as to minimize hydrophobic interactions.

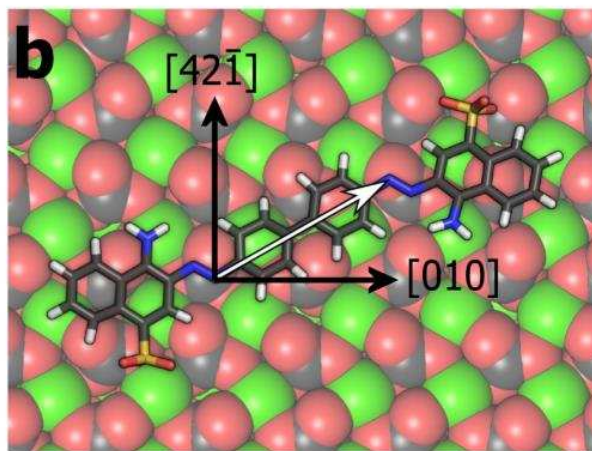
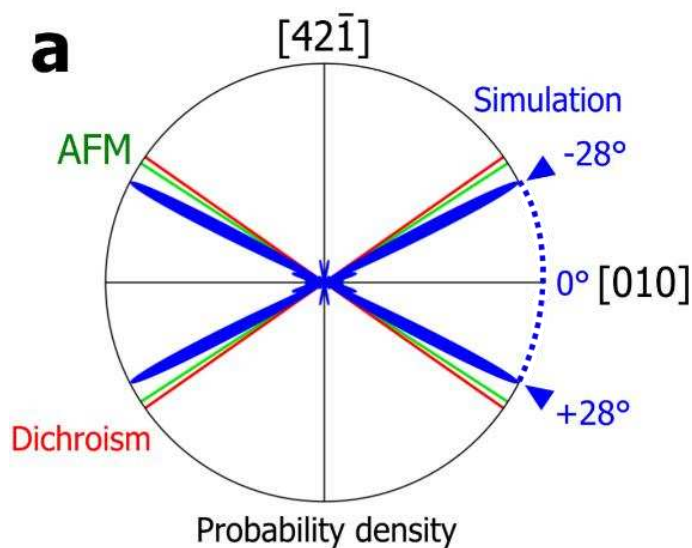


**Figure 5: Molecular simulation of Congo red at the calcite (104)/ water interface. (a)**

Canonical probability density for the orientation of the long axis of Congo red with respect to the calcite surface, computed using molecular simulation. Red arrows highlight the peaks at 34° to [010]. **(b)** A simulation snapshot of Congo red adsorbed at the interface (water not rendered for clarity) and aligned at ~34°. Atoms shown are Ca (green), O (red), S (yellow), C (grey), H (white).

### 3. Discussion

The influence of organic additives on calcite morphology has been extensively studied.<sup>1, 2</sup> While the more exotic morphologies, such as fibers and thin films, form *via* an amorphous precursor phase,<sup>55, 56</sup> the less remarkable morphology changes seen in single crystals can usually be directly linked to the molecular-scale interactions of the additives with the crystal surfaces.<sup>47</sup> These morphological changes are often accompanied by incorporation of the additives within the crystal,<sup>21, 29, 45</sup> but the mechanism of incorporation and location of the additives within the resulting composite can be challenging to study. For calcite, much information about the occlusion of small molecules and organic macromolecules has come from high resolution single-crystal and powder X-ray diffraction studies of biominerals and synthetic crystals. Anisotropic lattice distortions are typically observed, which can be attributed to the occluded additives.<sup>25, 41-</sup>  
<sup>43</sup> However, as calcite is itself anisotropic and most easily distorted along the *c*-axis,<sup>57</sup> it can be difficult to use these distortions to determine the placement of an additive within the crystal structure. A notable exception is a study where simulations of amino acids incorporated within calcite correctly predicted the lattice strains obtained by powder XRD.<sup>21</sup> Large additives, however, are not suitable for such analyses.

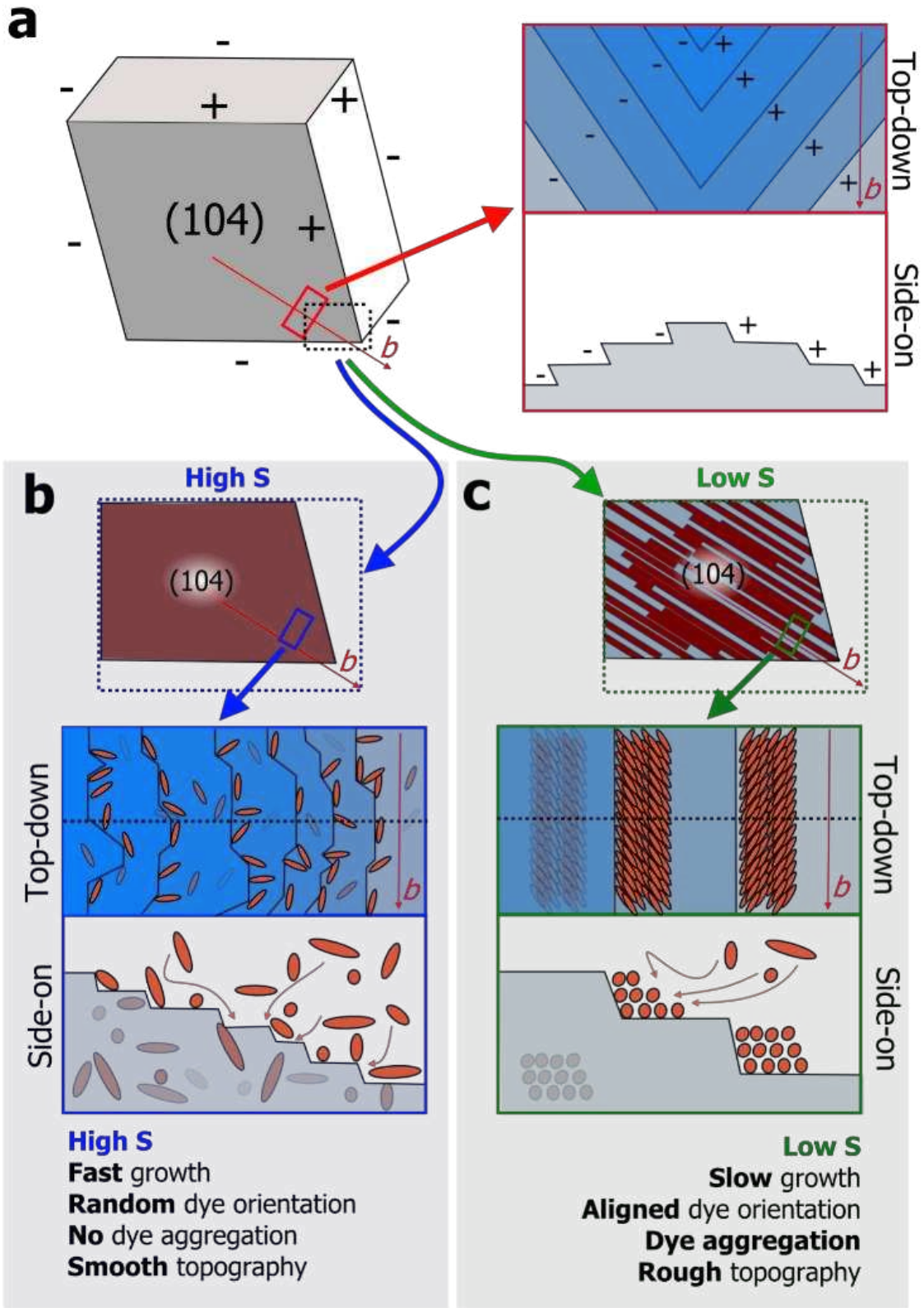


**Figure 6: Origins of growth condition-dependent observations of dichroism.** (a) Schematic representation of a calcite seed labelled with the (104) facet, [010], or *b*, zone axis; and corresponding acute (-) and obtuse (+) edge morphology. A schematic representation of an idealized two-dimensional growth island (red box) is shown in top-down and side-on views. (b and c) Schematic representations of a calcite surface - corresponding to the black dashed box in a - after overgrowth in the presence of Congo red at high S (b) and low S (c). The surface interaction and incorporated state of Congo red (red ovals) on two-dimensional growth islands under high S (blue box, b) and low S (green box, c) overgrowth conditions is shown. Congo red binds preferentially with obtuse steps in both configurations, but as single molecules with a random orientation at high S (b), and as aggregates oriented along [010] at low S (c). Step pinning by kink site binding at high S (b) is contrasted by macroscopic step pile-up caused by Congo red aggregates at low S (c). The orientation in both configurations is preserved upon incorporated. Note: in both b and c, the unrestricted propagation of acute steps is assumed, and therefore only slow growing obtuse steps are shown.

Dye molecules therefore provide a unique opportunity to study additive/crystal interactions. Upon incorporation, their distribution within the crystal is readily observable, and the optical properties of the resulting composite can reveal orientations.<sup>40</sup> By combining this information with an understanding of adsorption at the surface—e.g., obtained from AFM, an analysis of morphology and surface topography, molecular simulation, and other methods—the sequence of events from adsorption to occlusion can potentially be reconstructed.

The effects of Congo red on the gross morphology of calcite are consistent with preferential binding to the obtuse over the acute steps, akin to the modification produced by poly(styrene sulfonate).<sup>48</sup> The pronounced striations on the crystal surfaces (Figure 2) are then indicative of substantial binding of Congo red to the terraces along <010>, inhibiting overgrowth and

producing the pile-up of steps responsible for the striations. Both features were confirmed by *in situ* AFM. The Congo red aggregated on the {104} terraces to form tape-like islands. The orientation of these tapes parallel to the [010] ultimately causes the obtuse steps to be replaced with striations parallel to the [010] (Figure 3c). These supramolecular aggregates were previously shown by Momper et al.<sup>58</sup> to be organized with a periodic internal structure. One of the basis vectors was found at approximately 33° to [010], the relevance of which will be discussed below. The linear dichroism was correlated with the roughening of the crystal surface (Figure 4), as it presumably arises from Congo red aggregates. The significance of growth conditions in both cases, therefore, is that the rate of crystal growth limits the time available for dye aggregation at the steps, which then limits the degree of surface roughening and the collinear organization of the dyes (Figure 6). This account inspired a simple mathematical model in which the orientation of an occluding dye is assumed isotropic unless some stochastic event (aggregation) occurs before the local step advances far enough to preserve the prevailing orientation of the dye. The model predicts a sigmoidal dependence of the dichroic ratio on the log-supersaturation and provided a reasonably good fit to the experimental data (blue curve in Figure 4c).

The plateau in dichroic ratio at low supersaturation indicates that the dyes are maximally co-aligned. It can then be computed from the saturated dichroic ratio ( $R=1.97$ ) that the overgrown dyes are aligned at approximately 35° to the [010] axis. This striking similarity to the 33° angle reported by Momper *et al.*<sup>58</sup> not only substantiates our explanation but reveals that the orientation adopted by the dyes on the surface is preserved upon occlusion. To identify the significance of the 33-35° inclination, molecular simulations of a single Congo red molecule

adsorbed at the calcite (104)/water interface were performed, where the free energy as a function of the dye's orientation was computed with an enhanced sampling method. The simulations produced a canonical probability distribution that singled out an orientation of the Congo red biphenyl axis at  $28^\circ$  to [010] (Figure 5a). This is close enough to the orientations predicted by the AFM and optical analyses to strongly suggest that the Congo red dyes aggregate in a way that minimizes their free energy interaction with the underlying terrace.

In summary, the absence of dichroism at high supersaturation reveals that Congo red is overgrown with a random orientation during fast crystal growth (Figure 6b). This is likely because the steps are rough, and the dye orientation is influenced by the local kink configuration. Slower crystal growth allows the Congo red sufficient time to aggregate, yielding islands and the resultant surface striations (Figure 6c). The dye molecules organize within the islands, seemingly to minimize the dye-terrace free energy, and the crystal engulfs them so as to preserve that orientation. The structure of the occluded dye molecules can thus be rationalized by thermodynamics operating at the adsorption stage.

#### **4. Conclusions**

Soluble dye molecules provide a unique opportunity to investigate additive incorporation into crystals, where simple, non-destructive optical microscopy can reveal the direction of alignment of oriented dyes with respect to the crystal lattice. We have here applied this strategy to the growth of calcite, where despite being one of the most-studied crystals, there are few reports of its growth in the presence of dyes.<sup>59, 60</sup> The dichroism introduced by Congo red into calcite, when

combined with an analysis of surface adsorption, provided a novel means of following the entire process from adsorption to occlusion. Our results show that the adsorbed dyes have time to explore configuration space and achieve a local equilibrium prior to incorporation, upon which their orientation is preserved. This is important as it justifies the use of equilibrium models to study surface adsorption even under growth conditions and reveals that the incorporated state of macromolecules can be understood via thermodynamics at the surface. We suggest that dyes, and their associated dichroism in crystals, can play a significant role in elucidating additive/calcite interactions, where occlusion can be used to introduce new properties to the host crystal including color,<sup>26</sup> luminescence,<sup>38, 39, 61</sup> enhanced mechanical properties<sup>15, 21</sup> and stability,<sup>32</sup> and even changing the band-gap of semiconductor materials.<sup>62</sup>

## 5. Methods Section

A brief summary of key methods is provided here, and a detailed description is given in the Supporting Information.

*Overgrowth of Seed Crystals.* Overgrowth of calcite seeds with calcite/Congo red was conducted by placing calcite seeds in a supersaturated solution comprising  $[\text{CaCl}_2] = [\text{NaHCO}_3] = 4 \text{ mM}$ , 5 mM or 10 mM and Congo red (20  $\mu\text{M}$ ). 50-100  $\mu\text{m}$ -sized synthetic calcite crystals supported on glass cover slips were used as seeds. The overgrown crystals were then rinsed with water, bleached with NaOCl solution (11-14%) for 5 min, and washed again with DI water and ethanol. No amorphous calcium carbonate (ACC) precursor phase is produced and little *de novo* crystal precipitation occurs.

*De Novo Precipitation of Calcite/Congo Red Crystals.* Crystals were precipitated using the ammonia diffusion method (ADM),<sup>51</sup> the Kitano method<sup>52</sup> or by a direct mixing method. The ADM method was carried out by incubating a Petri dish containing cleaned glass cover slips and an aqueous solution of CaCl<sub>2</sub> (10 mM) and Congo red (20 μM) in a desiccator with a Petri dish filled with solid ammonium carbonate. The reaction was allowed to proceed for 3 days. Association of Ca<sup>2+</sup> ions with the Congo red molecules is apparent in a color change in a solution of Congo Red from X to Y on addition of Ca<sup>2+</sup> ions. The Kitano method was conducted by precipitating calcite from a filtered Ca(HCO<sub>3</sub>)<sub>2</sub> solution, where enough volume of Congo red stock solution was added to yield a dye concentration of 20 μM. The Petri dish was then sealed and punctured once to allow the effusion of gas over 16 h. The direct mixing method was conducted by precipitating crystals from an aqueous solution of [CaCl<sub>2</sub>] = [Na<sub>2</sub>CO<sub>3</sub>] = 5 mM and Congo red (20 μM), and isolating the glass cover slips supporting the crystals after 16 h. In all cases, once the reaction was complete the calcite-loaded glass substrates were rinsed with water, bleached with NaOCl solution (11-14%) for 5 min, and then washed again with DI water and ethanol.

*Image Analysis.* Analysis was conducted using ImageJ on a uniform region of interest within each crystal. For each micrograph and color, the mean value was determined, and plotted against the angle from which the micrograph was obtained. The relative red intensity, *I*, was calculated using

Equation 1:

$$I = \frac{I_{red}}{I_{red} + I_{green} + I_{blue}} \quad \text{Equation 1}$$

where *I<sub>red</sub>*, *I<sub>green</sub>* and *I<sub>blue</sub>* are RGB values (mean) obtained for red, green and blue, respectively.

*Optical Spectroscopy.* Absorbance spectra of calcite/Congo red crystals were obtained using a Nikon Eclipse LV100 microscope, where the camera was replaced by a single fiber optic leading to an Avantes spectrometer. The microscope was set to transmission mode with a 100× oil-immersion objective and a linear Nikon polarizer placed over the light source. Absorbance values at the absorbance maximum at 500 nm were used to calculate a dichroic ratio,  $R$ , using Equation 2:

$$R = \frac{A_{\parallel}^{500}}{A_{\perp}^{500}} \quad \text{Equation 2}$$

Dichroic ratio,  $R$ , represents a *maximum* change in the absorbance, where  $A_{\parallel}^{500}$  is the absorbance when the plane of polarised light is parallel to calcite's [010] axis, and therefore at a maximum; and  $A_{\perp}^{500}$  is the absorbance when the plane of polarized light is perpendicular to calcite's [010] axis, and therefore at a minimum. However, a ratio,  $A_n$ , can be calculated at any angle,  $n$ , giving a value  $1 < A_n < R$ , using Equation 3.

$$A_n = \frac{A_n^{500}}{A_{\perp}^{500}} \quad \text{Equation 3}$$

Here,  $A_n$  is the relative absorbance at 500 nm at any angle,  $n$ , compared to the absorbance when the plane of polarized light is perpendicular to calcite's [010] axis,  $A_{\perp}^{500}$ .

*Molecular Simulation.* The free energy as a function of the orientation of a single Congo red molecule adsorbed at the calcite (104)/water interface was obtained using umbrella sampling. The dye was initiated in direct contact with the calcite surface but was promptly displaced by the water, thus binding to the surface via shared solvent. This indirect binding eliminated the need to explicitly drive surface dehydration. The vector that connects the *ipso* N atoms of two azo groups

attached to the biaryl linker in the dye was projected onto the (104) surface and the subtended angle was taken as the collective variable. The umbrella sampling involved tethering the orientation of the dye with a harmonic potential ( $k = 3,923 \text{ kcal mol}^{-1} \text{ rad}^{-2}$ ) to a series of windows separated by  $2^\circ$  spanning the entire  $360^\circ$  range, then repeating with the dye adsorbed on its other face and combining the two free energy curves via an average of the Boltzmann probabilities. Note that, in practice, the symmetry of the system was exploited such that only a  $180^\circ$  range had to be sampled with the dye lying on a single face. The slow rotational kinetics meant that the configuration space had to be explored for a total of  $\sim 40$  ns per window to ensure convergence. The free energy itself was then constructed using the weighted histogram analysis method.<sup>63</sup> The histogram for each simulation window, as well as the resulting free energy curve, can both be seen in Figure S9. The canonical probability density  $\exp(-G/kT)$  shown in Figure 5a was computed from this free energy curve.

The molecular dynamics simulations were performed using LAMMPS modified with an in-house code for the umbrella sampling. The force fields were as described in Nalbach *et al*,<sup>54</sup> except a C-C-N=N dihedral of the CHARMM form<sup>64</sup> with an energy parameter of 2 kcal/mol was added to keep the azo groups in-plane. Integration was performed in the canonical ensemble using velocity Verlet with a 1 fs timestep. A Nosé-Hoover thermostat with a damping parameter of 100 fs was used to maintain a 300 K temperature. Long-range electrostatics were evaluated using PPPM with a tolerance of  $10^{-4}$ . A pair of sodium counterions were included to neutralize the charge of the dye.

*Computing Dye Orientation from Dichroic Ratio.* If the probability distribution  $p(\theta)$  is known for the orientation  $\theta$  of dyes occluded within the crystal then a dimensionless absorbance can be computed as a function of the orientation  $\phi$  of the optical polarization plane as follows,

$$A(\phi) = \int_0^{2\pi} p(\theta) \cos^2(\theta - \phi) d\theta \quad \text{Equation 4}$$

which follows from Malus's law. Since the dichroic ratio is also dimensionless, it can be recovered immediately from the dimensionless absorbance,

$$R = \frac{\max_{\phi} A(\phi)}{\min_{\phi} A(\phi)} \quad \text{Equation 5}$$

If all of the dyes are aligned along the same (or symmetrically equivalent) direction  $\theta_0$  then the probability density will take the form of a Dirac delta function  $p(\theta) = \delta(\theta - \theta_0)$ . Utilizing equations 4 and 5 as well as the combined symmetry of the calcite/Congo red system, the dye orientation can be recovered from the dichroic ratio as follows

$$\theta_0 = \frac{1}{2} \arccos\left(\frac{R-1}{R+1}\right) \quad \text{Equation 6}$$

where  $\theta_0$  is measured with respect to the  $\langle 010 \rangle$  axis.

*Dichroic Ratio Dependence on Supersaturation.* Consider a simple model where dye molecules adsorb to a crystal step but cannot dissolve, *i.e.* occlusion is inevitable, where occlusion is characterized by the step advancing a certain distance  $x$  and engulfing the dye. In the time interval between adsorption and occlusion, a second dye may adsorb next to the first, forming an aggregate. This event is assumed to be Poissonian with a characteristic timescale  $\tau$ . Upon occlusion, the molecules will have a uniformly random orientation unless it belongs to an

aggregate, in which case it will adopt a preferred orientation  $\theta_0$ . The probability distribution of the orientation of the dye at the moment of occlusion will then be

$$p(\theta) = \exp\left(-\frac{x}{v\tau}\right) \frac{1}{2\pi} + \left[1 - \exp\left(-\frac{x}{v\tau}\right)\right] \delta(\theta - \theta_0)$$

Equation 7

where  $v(S) = k(S - 1)\sqrt{S}$  is the step velocity, for a constant  $k$  and where the square-root term accounts for kink density.<sup>65</sup> Combining this with equations 4 and 5, the dichroic ratio takes the form

$$R(S) = \frac{1+r(S)}{1-r(S)} \quad \text{Equation 8}$$

where

$$r(S) = \left[1 - \exp\left(-\frac{b}{(S-1)\sqrt{S}}\right)\right] \cos(2\theta_0) \quad \text{Equation 9}$$

and  $b = x/(k\tau)$  is a dimensionless parameter. Taking  $\theta_0 = 35^\circ$ , a fit to experimental data gives  $b = 14$ . Approximating  $x \sim 1\text{nm}$  and  $k \sim 10\text{nm/s}$ ,<sup>66</sup> it follows that the aggregation time-scale is on the order of several milliseconds.

## **ASSOCIATED CONTENT**

**Supporting Information.** Materials; further information about sample preparation and characterization methods; supplementary table 1; and supplementary figures S1-S9. This material is available free of charge via the Internet at <http://pubs.acs.org>.” **Supporting Data.** Data supporting the findings of this study are available in the Research Data Leeds Repository with the identifier [<http://doi.org/10.5518/XX>].<sup>67</sup>

## **AUTHOR INFORMATION**

### **Corresponding Author**

\* F.Meldrum@leeds.ac.uk, david.green@hh.se and R.Darkins@ucl.ac.uk

### **Present Addresses**

† School of Business, Innovation and Sustainability, Halmstad University, Kristian IV:s väg 3, 301 18 Halmstad, Sweden

§ School of Natural Sciences, University of Central Lancashire, Preston, PR1 2HE, United Kingdom.

### **Author Contributions**

The manuscript was written through contributions of all authors. ‡These authors contributed equally.

### **Funding Sources**

We acknowledge the Engineering and Physical Sciences Research Council (EPSRC) Programme Grant (grant EP/R018820/1) which funds the Crystallization in the Real World consortium. This

project was also supported by EPSRC grants EP/P005241/1 and EP/M003027/1. We extend our thanks to the UKRI-STFC-Central laser facility at RCaH for access to the Octopus facility under proposal 17330015.

## **ABBREVIATIONS**

ADM, ammonia diffusion method; AFM, atomic force microscopy; CLFM, confocal laser scanning microscopy; DM, direct method; XRD, X-ray diffraction

## REFERENCES

- (1) Song, R.-Q.; Colfen, H., Additive controlled crystallization. *CrystEngComm* **2011**, *13*, 1249-1276.
- (2) Meldrum, F. C.; Colfen, H., Controlling Mineral Morphologies and Structures in Biological and Synthetic Systems. *Chem. Rev.* **2008**, *108*, 4332-4432.
- (3) Shtukenberg, A. G.; Lee, S. S.; Kahr, B.; Ward, M. D., Manipulating Crystallization with Molecular Additives. In *Ann. Rev. Chem. Biomol. Eng.*, Prausnitz, J. M.; Doherty, M. F.; Segalman, R. A., Eds. 2014; Vol. 5, pp 77-96.
- (4) Elhadj, S.; Salter, E. A.; Wierzbicki, A.; De Yoreo, J. J.; Han, N.; Dove, P. M., Peptide controls on calcite mineralization: Polyaspartate chain length affects growth kinetics and acts as a stereochemical switch on morphology. *Cryst. Growth Des.* **2006**, *6*, 197-201.
- (5) De Yoreo, J. J.; Vekilov, P. G., Principles of crystal nucleation and growth. *Rev. Mineral. Geochem.* **2003**, *54*, 57-93.
- (6) Wasylenki, L. E.; Dove, P. M.; Wilson, D. S.; De Yoreo, J. J., Nanoscale effects of strontium on calcite growth: An in situ AFM study in the absence of vital effects. *Geochim. Cosmochim. Acta* **2005**, *69*, 3017-3027.
- (7) Davis, K. J.; Dove, P. M.; Wasylenki, L. E.; De Yoreo, J. J., Morphological consequences of differential Mg<sup>2+</sup> incorporation at structurally distinct steps on calcite. *Am. Mineral.* **2004**, *89*, 714-720.
- (8) Dandekar, P.; Kuvadia, Z. B.; Doherty, M. F., Engineering Crystal Morphology. In *Ann. Rev. Mater. Res.*, Clarke, D. R., Ed. 2013; Vol. 43, pp 359-386.

- (9) Addadi, L.; Weiner, S., Interactions between acidic proteins and crystals: stereochemical requirements in biomineralization. *Proc. Natl. Acad. Sci. U.S.A.* **1985**, *82*, 4110-4114.
- (10) Albeck, S.; Addadi, L.; Weiner, S., Regulation of calcite crystal morphology by intracrystalline acidic proteins and glycoproteins. *Connec. Tiss. Res.* **1996**, *35*, 365-370.
- (11) Didymus, J. M.; Oliver, P.; Mann, S.; Devries, A. L.; Hauschka, P. V.; Westbroek, P., Influence of Low Molecular Weight and Macromolecular Organic Additives on the Morphology of Calcium Carbonate. *J. Chem. Soc. Faraday Trans.* **1993**, *89*, 2891-2900.
- (12) Tang, Y. M.; Zhang, F.; Cao, Z. Y.; Jing, W. H.; Chen, Y. Z., Crystallization of CaCO<sub>3</sub> in the presence of sulfate and additives: Experimental and molecular dynamics simulation studies. *J. Coll. Int. Sci.* **2012**, *377*, 430-437.
- (13) Ukrainczyk, M.; Stelling, J.; Vucak, M.; Neumann, T., Influence of etidronic acid and tartaric acid on the growth of different calcite morphologies. *J. Cryst. Growth* **2013**, *369*, 21-31.
- (14) Cho, K. R.; Kim, Y. Y.; Yang, P. C.; Cai, W.; Pan, H. H.; Kulak, A. N.; Lau, J. L.; Kulshreshtha, P.; Armes, S. P.; Meldrum, F. C.; De Yoreo, J. J., Direct observation of mineral-organic composite formation reveals occlusion mechanism. *Nat. Commun.* **2016**, *7*, 10187.
- (15) Kim, Y. Y.; Ganesan, K.; Yang, P. C.; Kulak, A. N.; Borukhin, S.; Pechook, S.; Ribeiro, L.; Kroger, R.; Eichhorn, S. J.; Armes, S. P.; Pokroy, B.; Meldrum, F. C., An artificial biomineral formed by incorporation of copolymer micelles in calcite crystals. *Nat. Mater.* **2011**, *10*, 890-896.
- (16) Dunlop, J. W. C.; Fratzl, P., Biological Composites. In *Ann. Rev. Mater. Res.*, Clarke, D. R.; Ruhle, M.; Zok, F., Eds. 2010; Vol. 40, pp 1-24.
- (17) Paquette, J.; Reeder, R. J., New type of compositional zoning in calcite: Insights into crystal-growth mechanisms. *Geol.* **1990**, *18*, 1244-7.

(18) Paquette, J.; Reeder, R. J., Relationship between surface structure, growth mechanism, and trace element incorporation in calcite. *Geochim. Cosmochim. Acta* **1995**, *59*, 735-49.

(19) Reeder, R. J.; Paquette, J., Sector Zoning in Natural and Synthetic Calcites. *Sed. Geol.* **1989**, *65*, 239-247.

(20) Borukhin, S.; Bloch, L.; Radlauer, T.; Hill, A. H.; Fitch, A. N.; Pokroy, B., Screening the Incorporation of Amino Acids into an Inorganic Crystalline Host: the Case of Calcite. *Adv. Func. Mater.* **2012**, *22*, 4216-4224.

(21) Kim, Y. Y.; Carloni, J. D.; Demarchi, B.; Sparks, D.; Reid, D. G.; Kunitake, M. E.; Tang, C. C.; Duer, M. J.; Freeman, C. L.; Pokroy, B.; Penkman, K.; Harding, J. H.; Estroff, L. A.; Baker, S. P.; Meldrum, F. C., Tuning hardness in calcite by incorporation of amino acids. *Nat. Mater.* **2016**, *15*, 903-910.

(22) Green, D. C.; Ihli, J.; Kim, Y. Y.; Chong, S. Y.; Lee, P. A.; Empson, C. J.; Meldrum, F. C., Rapid Screening of Calcium Carbonate Precipitation in the Presence of Amino Acids: Kinetics, Structure, and Composition. *Cryst. Growth Des.* **2016**, *16*, 5174-5183.

(23) Su, X.; Kamat, S.; Heuer, A. H., The structure of sea urchin spines, large biogenic single crystals of calcite. *J. Mater. Sci.* **2000**, *35*, 5545-5551.

(24) Robach, J. S.; Stock, S. R.; Veis, A., Transmission electron microscopy characterization of macromolecular domain cavities and microstructure of single-crystal calcite tooth plates of the sea urchin *Lytechinus variegatus*. *J. Struc. Biol.* **2005**, *151*, 18-29.

(25) Berman, A.; Hanson, J.; Leiserowitz, L.; Koetzle, T. F.; Weiner, S.; Addadi, L., Biological Control of Crystal Texture: A Widespread Strategy for Adapting Crystal Properties to Function. *Science* **1993**, *259*, 776-779.

(26) Kulak, A. N.; Yang, P. C.; Kim, Y. Y.; Armes, S. P.; Meldrum, F. C., Colouring crystals with inorganic nanoparticles. *Chem. Commun.* **2014**, *50*, 67-69.

(27) Kulak, A. N.; Semsarilar, M.; Kim, Y. Y.; Ihli, J.; Fielding, L. A.; Cespedes, O.; Armes, S. P.; Meldrum, F. C., One-pot synthesis of an inorganic heterostructure: uniform occlusion of magnetite nanoparticles within calcite single crystals. *Chem. Sci.* **2014**, *5*, 738-743.

(28) Kim, Y.-Y.; Darkins, R.; Broad, A.; Kulak, A. K.; Holden, M. A.; Nahi, O.; Armes, S. P.; Tang, C. C.; Thompson, R. F.; Marin, F.; Duffy, D. M.; Meldrum, F. C., Hydroxyl-Rich Macromolecules Enable the Bio-Inspired Synthesis of Single Crystal Nanocomposites. *Nat. Commun.* **2019**, 5682.

(29) Kim, Y. Y.; Ribeiro, L.; Maillot, F.; Ward, O.; Eichhorn, S. J.; Meldrum, F. C., Bio-Inspired Synthesis and Mechanical Properties of Calcite-Polymer Particle Composites. *Adv. Mater.* **2010**, *22*, 2082-2086.

(30) Kim, Y. Y.; Semsarilar, M.; Carloni, J. D.; Cho, K. R.; Kulak, A. N.; Polishchuk, I.; Hendley, C. T.; Smeets, P. J. M.; Fielding, L. A.; Pokroy, B.; Tang, C. C.; Estroff, L. A.; Baker, S. P.; Armes, S. P.; Meldrum, F. C., Structure and Properties of Nanocomposites Formed by the Occlusion of Block Copolymer Worms and Vesicles Within Calcite Crystals. *Adv. Func. Mater.* **2016**, *26*, 1382-1392.

(31) Ning, Y.; Han, L. J.; Derry, M. J.; Meldrum, F. C.; Armes, S. P., Model Anionic Block Copolymer Vesicles Provide Important Design Rules for Efficient Nanoparticle Occlusion within Calcite. *J. Am. Chem. Soc.* **2019**, *141*, 2557-2567.

(32) Liu, M. X.; Chen, Y. L.; Tan, C. S.; Quintero-Bermudez, R.; Proppe, A. H.; Munir, R.; Tan, H. R.; Voznyy, O.; Scheffel, B.; Walters, G.; Kam, A. P. T.; Sun, B.; Choi, M. J.; Hoogland, S.; Amassian, A.; Kelley, S. O.; de Arquer, F. P. G.; Sargent, E. H., Lattice anchoring stabilizes solution-processed semiconductors. *Nature* **2019**, *570*, 96-101.

(33) Liu, Y. J.; Yuan, W. T.; Shi, Y.; Chen, X. Q.; Wang, Y.; Chen, H. Z.; Li, H. Y., Functionalizing Single Crystals: Incorporation of Nanoparticles Inside Gel-Grown Calcite Crystals. *Angew. Chem. Int. Ed.* **2014**, *53*, 4127-4131.

(34) Li, H.; Xin, H. L.; Muller, D. A.; Estroff, L. A., Visualizing the 3D Internal Structure of Calcite Single Crystals Grown in Agarose Hydrogels. *Science* **2009**, *326*, 1244-1247.

(35) Ihli, J.; Levenstein, M. A.; Kim, Y.-Y.; Wakonig, K.; Ning, Y.; Tatani, A.; Kulak, A. N.; Green, D. C.; Holler, M.; Armes, S. P.; Meldrum, F. C., Ptychographic X-ray Tomography Reveals Additive Zoning in Nanocomposite Single Crystals. *Chem. Sci.* **2020**, *11*, 355-363.

(36) Schenk, A. S.; Zlotnikov, I.; Pokroy, B.; Gierlinger, N.; Masic, A.; Zaslansky, P.; Fitch, A. N.; Paris, O.; Metzger, T. H.; Colfen, H.; Fratzl, P.; Aichmayer, B., Hierarchical Calcite Crystals with Occlusions of a Simple Polyelectrolyte Mimic Complex Biomineral Structures. *Adv. Func. Mater.* **2012**, *22*, 4668-4676.

(37) Weber, E.; Bloch, L.; Guth, C.; Fitch, A. N.; Weiss, I. M.; Pokroy, B., Incorporation of a Recombinant Biomineralization Fusion Protein into the Crystalline Lattice of Calcite. *Chem. Mater.* **2014**, *26*, 4925-4932.

(38) Green, D. C.; Holden, M. A.; Levenstein, M. A.; Zhang, S. H.; Johnson, B. R. G.; de Pablo, J. G.; Ward, A.; Botchway, S. W.; Meldrum, F. C., Controlling the fluorescence and room-temperature phosphorescence behaviour of carbon nanodots with inorganic crystalline nanocomposites. *Nature Commun.* **2019**, *10*, 206.

(39) Liu, Y. J.; Zang, H. D.; Wang, L.; Fu, W. F.; Yuan, W. T.; Wu, J. K.; Jin, X. Y.; Han, J. S.; Wu, C. F.; Wang, Y.; Xing, H. L. L.; Chen, H. Z.; Li, H. Y., Nanoparticles Incorporated inside Single-Crystals: Enhanced Fluorescent Properties. *Chem. Mater.* **2016**, *28*, 7537-7543.

- (40) Kahr, B.; Gurney, R. W., Dyeing crystals. *Chem. Revs.* **2001**, *101*, 893-951.
- (41) Pokroy, B.; Fitch, A. N.; Zolotoyabko, E., The microstructure of biogenic calcite: A view by high-resolution synchrotron powder diffraction. *Adv. Mater.* **2006**, *18*, 2363-2368.
- (42) Aizenberg, J.; Hanson, J.; Koetzle, T. F.; Leiserowitz, L.; Weiner, S.; Addadi, L., Biologically Induced Reduction in Symmetry: A Study of Crystal Texture of Calcitic Sponge Spicules. *Chem. Eur. J.* **1995**, *1*, 414-422.
- (43) Pokroy, B.; Fitch, A. N.; Marin, F.; Kapon, M.; Adir, N.; Zolotoyabko, E., Anisotropic lattice distortions in biogenic calcite induced by intra-crystalline organic molecules. *J. Struc. Biol.* **2006**, *155*, 96-103.
- (44) Kahr, B.; Shtukenberg, A. G., Dyeing crystals since 2000. *Crystengcomm* **2016**, *18*, 8988-8998.
- (45) Green, D. C.; Ihli, J.; Thornton, P. D.; Holden, M. A.; Marzec, B.; Kim, Y. Y.; Kulak, A. N.; Levenstein, M. A.; Tang, C.; Lynch, C.; Webb, S. E. D.; Tynan, C. J.; Meldrum, F. C., 3D visualization of additive occlusion and tunable full-spectrum fluorescence in calcite. *Nature Commun.* **2016**, *7*, 13524.
- (46) Benedict, J. B.; Cohen, D. E.; Lovell, S.; Rohl, A. L.; Kahr, B., What is syncrystallization? States of the pH indicator methyl red in crystals of phthalic acid. *J. Am. Chem. Soc.* **2006**, *128*, 5548-5559.
- (47) Orme, C. A.; Noy, A.; Wierzbicki, A.; McBride, M. T.; Grantham, M.; Teng, H. H.; Dove, P. M.; DeYoreo, J. J., Formation of chiral morphologies through selective binding of amino acids to calcite surface steps. *Nature* **2001**, *411*, 775-779.

- (48) Smeets, P. J. M.; Cho, K. R.; Sommerdijk, N.; De Yoreo, J. J., A Mesocrystal-Like Morphology Formed by Classical Polymer-Mediated Crystal Growth. *Adv. Func. Mater.* **2017**, *27*, 1701658.
- (49) Edwards, R. A.; Woody, R. W., Molecular Orbital Calculations of the Optical Properties of Congo Red and Cibacron Blue and their Complexes with Proteins. *J. Phys. Chem.* **1983**, *87*, 1329-1337.
- (50) Bullard, T.; Wustholz, K. L.; Bott, E. D.; Robertson, M.; Reid, P. J.; Kahr, B., Role of Kinks in Dyeing Crystals: Confocal Luminescence Microscopy from Single Molecules to Square Centimeters. *Cryst. Growth Des.* **2009**, *9*, 982-990.
- (51) Ihli, J.; Bots, P.; Kulak, A.; Benning, L. G.; Meldrum, F. C., Elucidating Mechanisms of Diffusion-Based Calcium Carbonate Synthesis Leads to Controlled Mesocrystal Formation. *Adv. Funct. Mater.* **2013**, *23*, 1965-1973.
- (52) Kitano, Y., The Behaviour of Various Inorganic Ions in the Separation of Calcium Carbonate from a Bicarbonate Solution. *Bull. Chem. Soc. Jn.* **1962**, *35*, 1973-1980.
- (53) Green, D. C.; Shida, Y.; Honma, N.; Holden, M. A.; Kim, Y.-Y.; Kulak, A. N.; Ogasawara, W.; Meldrum, F. C., Skin-Deep Surface Patterning of Calcite. *Chem. Mater.* **2019**, *31*, 8725–8733.
- (54) Nalbach, M.; Raiteri, P.; Klassen, S.; Schafer, S.; Gale, J. D.; Bechstein, R.; Kuhnle, A., Where Is the Most Hydrophobic Region? Benzopurpurine Self-Assembly at the Calcite-Water Interface. *J. Phys. Chem. C* **2017**, *121*, 24144-24151.
- (55) Gower, L. B., Biomimetic Model Systems for Investigating the Amorphous Precursor Pathway and Its Role in Biomineralization. *Chem. Revs.* **2008**, *108*, 4551-4627.

- (56) Cantaert, B.; Kim, Y.-Y.; Ludwig, H.; Nudelman, F.; Sommerdijk, N. A. J. M.; Meldrum, F. C., Think Positive: Phase Separation Enables a Positively Charged Additive to Induce Dramatic Changes in Calcium Carbonate Morphology. *Adv. Func. Mater.* **2012**, *22*, 907-915.
- (57) Bass, J. D., *Mineral Physics and Crystallography: A Handbook of Physical Constants*. ed.; American Geophysical Union: 2013.
- (58) Momper, R.; Nalbach, M.; Lichtenstein, K.; Bechstein, R.; Kuhnle, A., Stabilization of Polar Step Edges on Calcite (10.4) by the Adsorption of Congo Red. *Langmuir* **2015**, *31*, 7283-7287.
- (59) Kohlschütter, V.; Egg, C., *Helv. Chim. Acta* **1925**, *8*, 697-708.
- (60) Marzec, B.; Green, D. C.; Holden, M. A.; Coté, A. S.; Ihli, J.; Khalid, S.; Kulak, A.; Walker, D.; Tang, C.; Duffy, D. M.; Kim, Y.-Y.; Meldrum, F. C., Amino Acid-Assisted Incorporation of Dye Molecules within Calcite Crystals. *Angew. Chem. Int. Ed.* **2018**, *57*, 8623-8628.
- (61) Adam, M.; Erdem, T.; Stachowski, G. M.; Soran-Erdem, Z.; Lox, J. F. L.; Bauer, C.; Poppe, J.; Demir, L. V.; Gaponik, N.; Eychmuller, A., Implementation of High-Quality Warm-White Light-Emitting Diodes by a Model-Experimental Feedback Approach Using Quantum Dot-Salt Mixed Crystals. *ACS Appl. Mater. Int.* **2015**, *7*, 23364-23371.
- (62) Brif, A.; Ankonina, G.; Drathen, C.; Pokroy, B., Bio-Inspired Band Gap Engineering of Zinc Oxide by Intracrystalline Incorporation of Amino Acids. *Adv. Mater.* **2014**, *26*, 477-481.
- (63) Roux, B., The Calculation of the Potential of Mean Force using Computer Simulations. *Comp. Phys. Commun.* **1995**, *91*, 275-282.
- (64) MacKerell, A. D.; Bashford, D.; Bellott, M.; Dunbrack, R. L.; Evanseck, J. D.; Field, M. J.; Fischer, S.; Gao, J.; Guo, H.; Ha, S.; Joseph-McCarthy, D.; Kuchnir, L.; Kuczera, K.; Lau, F. T. K.; Mattos, C.; Michnick, S.; Ngo, T.; Nguyen, D. T.; Prodhom, B.; Reiher, W. E.; Roux, B.; Schlenkrich,

M.; Smith, J. C.; Stote, R.; Straub, J.; Watanabe, M.; Wiorcikiewicz-Kuczera, J.; Yin, D.; Karplus, M., All-atom empirical potential for molecular modeling and dynamics studies of proteins. *J. Phys. Chem. B* **1998**, *102*, 3586-3616.

(65) Voronkov, V. V., The movement of an elementary step by means of the formation of one-dimensional nuclei. *Phys. Cryst.* **1970**, *15*, 8–13.

(66) Teng, H. H.; Dove, P. M.; De Yoreo, J. J., Kinetics of calcite growth: Surface processes and relationships to macroscopic rate laws. *Geochim. Cosmochim. Acta* **2000**, *64*, 2255-2266.

(67) Green, D.C.; Dataset for Dichroic Calcite Reveals the Pathway from Additive Binding to Occlusion, *Research Data Leeds Repository*, **2016**, <http://doi.org/10.5518/XX>.

## For Table of Contents Only

Dichroic Calcite Reveals the Pathway from Additive Binding to Occlusion.

David C. Green<sup>a†\*</sup>, Robert Darkins<sup>b‡\*</sup>, Bartosz Marzec<sup>a</sup>, Mark A. Holden<sup>a,c§</sup>, Ian J. Ford<sup>b</sup>, Stanley W. Botchway<sup>d</sup>, Bart Kahre, Dorothy M. Duffy<sup>b</sup> and Fiona C. Meldrum<sup>a\*</sup>

Growth of calcite in the presence of Congo red yields unusual dichroic crystals whose optical properties reveal the organization of these organic additives within the crystal. In combination with information about additive binding obtained from *in situ* atomic force microscopy, molecular simulations and changes in crystal morphologies, new insight is obtained into the pathway from additive binding to occlusion.

